ISSN 1068-3755, Surface Engineering and Applied Electrochemistry, 2020, Vol. 56, No. 4, pp. 510–516. © Allerton Press, Inc., 2020.
Russian Text © The Author(s), 2019, published in Elektronnaya Obrabotka Materialov, 2019, No. 4, pp. 56–63.

Study into Synchronous Flows of Bactericidal Ultraviolet Radiation and Transition Oxides Metals (Zn, Cu, Fe) in a Pulsed Gas Discharge Overvoltage Reactor Nanosecond Discharge in the Air

A. K. Shuaibov[a], *, A. Y. Minya[a], A. A. Malinina[a], A. N. Malinin[a], Z. T. Gomoki[a], I. V. Shevera[a], and V. V. Danilo[a]

[a] *State Higher Educational Institution Uzhgorod National University, Uzhhorod, 88000 Ukraine*

* *e-mail: alexsander.shuaibov@uzhnu.edu.ua*

Received February 13, 2019; revised May 20, 2019; accepted May 20, 2019

Abstract—The characteristics of an overstressed, high-current nanosecond discharge in atmospheric air between zinc, copper, and iron electrodes are given with a distance between the electrodes of 1–3 mm. It is established that this discharge is a point source of ultraviolet radiation in the spectral range of 200–300 nm and a nanoparticle stream of zinc, copper, and iron oxides. The optimization results of the UV emitter depending on the pumping conditions and parameters of the discharge medium, as well as the optical characteristics of the film nanostructures of transition metal oxides deposited on the surface of a glass substrate, are presented.

Keywords: high-current nanosecond discharge, zinc, copper, iron, air, emission and transmission spectrum, metal oxide nanostructures, photoluminescence

DOI: 10.3103/S106837552004016X

INTRODUCTION

The use in biomedical engineering of gas-discharge sources of bactericidal ultraviolet (UV) radiation, such as lamps on vapors or amalgams of mercury, xenon, and inert gas halide molecules, has recently been significantly developed [1–3]. In addition to the factor of ultraviolet radiation for various applications in medicine, biology, and agricultural technologies, other factors of gas discharge (radicals), which are effectively formed in open plasma sources based on atmospheric pressure air, are important. Thus, the characteristics of a source based on a flare corona are given in [4]. Its use for plasma pretreatment of lettuce seeds showed that the germination rate of treated seeds increases by more than 25%. In [5], a barrier discharge with flat electrodes in atmospheric pressure air was successfully applied to inactivate microorganisms.

The characteristics of an open, overstretched nanosecond discharge in atmospheric pressure air between copper electrodes with an ecton mechanism for introducing copper vapor into the discharge gap were studied [6]. This discharge is a point source of ultraviolet radiation in the spectral range 200–230 nm. A more detailed study of this discharge revealed that, simultaneously with ultraviolet radiation, it is a source of a stream of copper oxides in the form of individual molecules or, more likely, clusters of different compositions that are deposited on a glass substrate in the form of nanostructured films [7, 8]. Nanostructures based on zinc and copper oxides are characterized by a pronounced antimicrobial effect [9–11], and magnetic nanostructures of iron oxides are promising for use as biological sensors [12] and a number of other medical applications [13].

Therefore, the development of new methods for the simultaneous production of bactericidal ultraviolet radiation and flows of nano-particles of transition metals, which will enhance the inactivation and antimicrobial properties of gas-discharge air plasma, are of considerable interest for applications in microbiology, medicine, and agricultural technologies.

This article discusses the design of a pulsed plasma-chemical reactor, provides the parameters and optical characteristics of a plasma of an overstressed nanosecond discharge between transition metal electrodes (Zn, Cu, Fe), and gives the results of studying the characteristics of transition metal oxide nanostructures.

DEVICE FOR DISCHARGE REACTOR. TECHNIQUE AND EXPERIMENTAL CONDITIONS

The design of a pulsed gas-discharge reactor based on a bipolar overstressed nanosecond discharge in atmospheric pressure air is shown in Fig. 1. Electrodes with a diameter of 5 mm and a length of 30 mm made

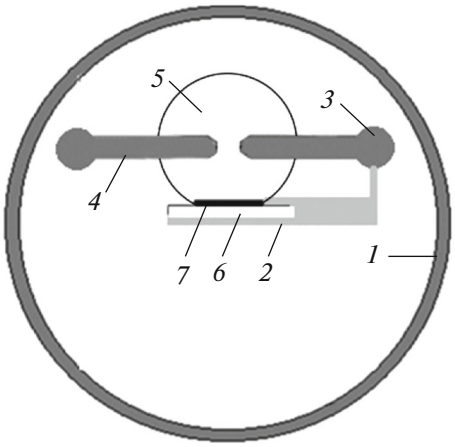

Fig. 1. Scheme of a pulsed plasma chemical reactor: (*1*) housing dielectric discharge chamber; (*2*) substrate fixation system for spraying thin films; (*3*) interelectrode distance control system; (*4*) metal electrodes; (*5*) film deposition zone; (*6*) glass substrate; (*7*) film.

of zinc, copper, or stainless steel were installed in a sealed chamber of a dielectric volume of 3 L. The radius of curvature of the electrodes' working end part was 3 mm. To reduce the influence of electromagnetic interference on the system for recording the characteristics of the discharge, a cell with a system of electrodes was installed in a screen of a metal grid. The discharge for all types of electrodes was studied at atmospheric air pressure.

To ignite the discharge, high voltage bipolar pulses with a total duration of 50–100 ns and an amplitude of ±(20–40) kV were applied to the metal electrodes. In this case, a uniform discharge was ignited between the tips of the electrodes with an amplitude of current pulses of 50–170 A [14, 15]. The plasma volume did not exceed 5–10 mm^3. At an interelectrode distance of 1–3 mm, the discharge gap was overstressed. In this mode of discharge ignition, favorable conditions were created for the ecton introduction of metal vapors from the surface of the electrodes, as in the article [6], where copper electrodes were used.

The voltage pulses at the discharge gap and the discharge current were measured using a broadband capacitive divider, Rogowski belt, and a 6-LOR 04 broadband oscilloscope. The temporal resolution of this recording system was 2–3 ns. The spatial characteristics of the discharge were studied using a digital camera. The pulse repetition rate varied in the range of f = 35–1000 Hz. The plasma radiation spectra were recorded using an MDR-2 monochromator, an FEU-106 photomultiplier, a direct current amplifier, and an electronic potentiometer. The radiation from the discharge plasma was analyzed in the spectral range 200–650 nm. The total relative power of the UV radiation of the discharge was measured in the spectral range 200–280 nm using an ultraviolet radiation power meter TKA-PKM. The radiation transmission spectra of thin nanostructured films that were deposited on glass substrates were recorded using an OCEAN OPTICS USB 2000 spectrometer. The probe radiation was applied to a film and a glass substrate using an optical fiber system.

The films were sprayed for 30–60 min when a glass substrate was installed at a distance of 30 mm from the center of the discharge gap, with an interelectrode distance of 1–3 mm, voltage pulse amplitude of ±20 kV, and pulse repetition rate of 40–100 Hz.

The surface image of thin nanostructured films was recorded using a Cross Beam Workstation Auriga scanning electron microscope (Carl Zeiss).

Raman scattering spectra were excited using an argon ion laser, which generated radiation at a wavelength of 514.5 nm. The Raman scattering spectra of thin films of transition metal oxides were studied using an nVia Renishaw spectrometer.

The photoluminescence spectra of the synthesized films were studied by irradiating the film with radiation from a high-pressure arc mercury lamp at different wavelengths in the 270–600-nm spectral range. In this case, the radiation of a mercury lamp in spectral intervals of 5 nm was released within fixed wavelengths using a separate monochromator and then sent to the film surface. The photoluminescence spectrum of nanostructures was recorded by a separate spectrophotometer.

CHARACTERISTICS AND PARAMETERS OF OVER-STRESSED NANOSECOND DISCHARGE

Let us consider the results of studying the characteristics and plasma parameters of an overstressed nanosecond discharge in air between electrodes of zinc, copper, and iron under the condition of micropoint explosions on the surface of the electrodes and the formation of the corresponding ectons. Photos of discharges at a pulse frequency repetition rate (f = 40–1000 Hz) for all types of electrodes (Zn, Cu, Fe) and their combination, when the distance between them was within 1–3 mm, were similar to those given for the discharge between copper electrodes [6, 13]. At discharge pulse repetition frequencies in the range of 35–150 Hz, the discharge had a diffuse form. The plasma diameter in the interelectrode gap was approximately equal to the interelectrode distance. At frequencies in the range of 400–1000 Hz, the diameter of the plasma of an overstressed nanosecond discharge increased by 3–4 times and covered new areas of the working surfaces of the electrodes. The causes of ignition of a fairly homogeneous diffuse discharge under the conditions of these experiments were considered in [6, 16].

Figure 2 shows the waveforms of voltage and current pulses for a discharge between electrodes made of copper and stainless steel. Similar waveforms were also

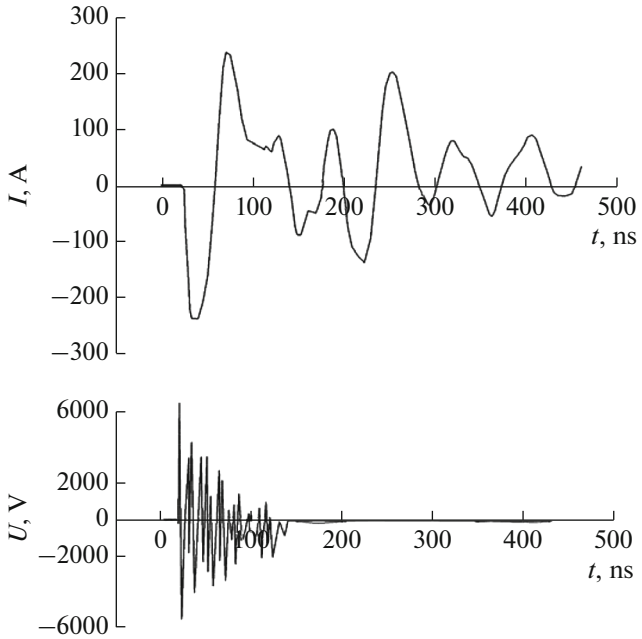

Fig. 2. Oscillograms of current and voltage of an overstressed nanosecond discharge in air between a copper electrode and a stainless-steel electrode (interelectrode distance $d = 3$ mm).

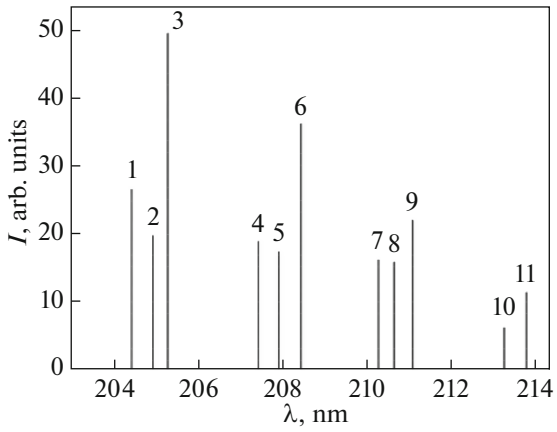

Fig. 3. Portion of the spectrum of the plasma radiation of a nanosecond discharge between zinc electrodes with the most intense spectral lines of zinc atoms and ions (d = 2 mm; f = 100 Hz).

obtained for discharges between electrodes of zinc, copper, and stainless steel. The duration of the main part of the train of voltage pulses reached 50–120 ns. The bipolar spikes of the voltage pulse had an amplitude of the positive and negative components up to 20–30 kV. The discharge current pulses consisted of a sequence of current pulses with an amplitude of positive and negative pulses of 120–150 A. The total length of a sequence of current pulses with an amplitude decreasing in time reached 150–200 ns. By graphically multiplying the waveforms of current pulses and voltage waveforms, the time distribution of the pulse contribution of energy to the plasma of the discharge under study was obtained. The maximum pulse discharge power was observed in the initial stage of the breakdown of the discharge gap and reached 2–4 MW. Time integration of pulsed power made it possible to determine the electrical energy that was introduced into the plasma of a nanosecond discharge during one sequence of voltage and current pulses. For the conditions of our experiments, the amount of energy that was deposited into the plasma in one pulse reached $E = 100$ mJ.

The ultraviolet radiation spectra of the plasma of the investigated discharge between the copper electrodes and the results of their identification are given in [6], and the emission spectra of discharges between zinc and stainless-steel electrodes are presented in Figs. 3 and 4. Approximately 90% of the plasma radiation power in the spectral range of 200–1000 nm for discharges between zinc and copper electrodes is concentrated in the spectral range of 200–260 nm. For overvoltage nanosecond discharge between copper electrodes, the spectral lines of copper ions were the main ones in the radiation spectrum; the spectral lines of zinc atoms and ions were the main ones in the UV emission spectra of the discharge between zinc electrodes: 202.6, 206.2 nm Zn(II); 250.2, 255.8 nm Zn(I). The results of the identification of the main spectral lines of atoms and iron ions that were observed in the discharge between stainless steel electrodes are given in Table 1.

Deciphering the emission spectra of iron plasma showed that the spectral lines of atoms and singly charged iron ions dominate in the discharge between stainless steel electrodes, and the spectral line of 249.6 nm Fe(I) was the most intense. Our results are in good agreement with the corresponding emission spectra of a high-voltage subnanosecond discharge in air atmospheric pressure for a needle–plane electrode system [17].

The plasma parameters of a nanosecond discharge for a mixture of copper and air vapors at atmospheric pressure (component ratio 30 Pa : 101 kPa, respectively) were determined numerically and calculated as full integrals of the electron energy distribution function (EEDF). EEDFs were found numerically by solving the Boltzmann kinetic equation in the binomial approximation. EEDF calculations were performed using the program [18]. Based on the obtained EEDFs, the average electron energy and electron mobility are determined. The ratio of the concentration of copper vapor and the gas concentration of a standard atmosphere at a pressure of 101 kPa argon, carbon dioxide, oxygen, and nitrogen was as follows: 0.3 : 7 : 0.27 : 159 : 599. The calculations were performed depending on the plasma parameters on the magnitude of the reduced electric field (the ratio of the

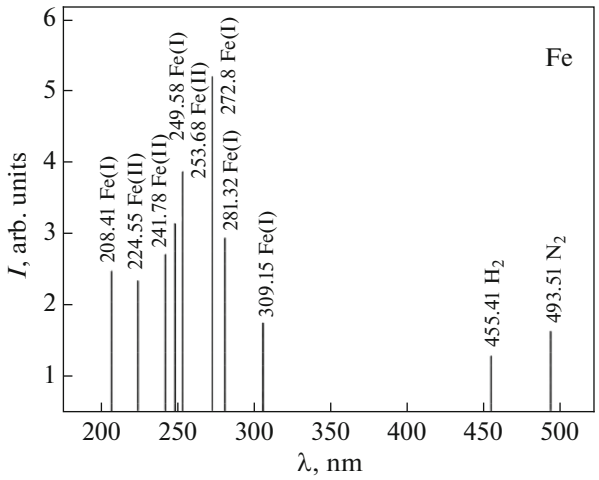

Fig. 4. Emission spectrum of a nanosecond plasma discharge in air between stainless steel electrodes (at $f = 40$ Hz).

electric field strength (E) to the total concentration of copper atoms, argon, and molecules of carbon dioxide, oxygen, and nitrogen (N)). Parameter change range $E/N = 1$–1300 Td (1×10^{-17}–1×10^{-15} V cm^2) included parameter values E/N, which were implemented in the experiment.

In the integral of collisions of electrons with atoms and molecules, the following processes are taken into account: elastic scattering of electrons by copper atoms; excitation of energy levels of copper atoms (threshold energies of 1500, 3800, 5100 eV); ionization of copper atoms (threshold energy 7.724 eV); elastic scattering of electrons by copper atoms; excitation of the energy level of argon atoms (threshold energy 11.50 eV); ionization of argon atoms (threshold energy of 15.80 eV); elastic scattering and excitation of energy levels of carbon dioxide molecules: vibrational (threshold energies 0.083, 0.167, 0.252, 0.291, 0.339, 0.422, 0.505, 2.5 eV), electronic (threshold energies: 7.0, 10.5 eV); dissociative electron attachment (threshold energy 3.85 eV); ionization (threshold energy 13.30 eV); elastic scattering and excitation of energy levels of oxygen molecules: vibrational (threshold energies 0.190, 0.380, 0.570, 0.750 eV), electronic (threshold energies 0.977, 1.627, 4.500, 6,000, 8.400, 9.970 eV); dissociative electron attachment (threshold energy 4.40 eV), ionization (threshold energy 12.06 eV); elastic scattering and excitation of energy levels of nitrogen molecules: rotational (threshold energy 0.020 eV), vibrational (threshold energy 0.290, 0.291, 0.590, 0.880, 1.170, 1.470, 1.760, 2.060, 2.350 eV), electronic (threshold energy 6.170, 7.000, 7.350, 7.360, 7.800, 8.160, 8.400, 8.550, 8.890, 11.03, 11.87, 12.25, 13.00 eV), ionization (threshold energy 15.60 eV). Data on the absolute values of the effective cross sections of these processes, as well as their dependences on electron energies, were taken from the database [18].

Electron concentration (N_e) was calculated according to the well-known formula [19]:

$$N_e = j/eV_{\text{dr}},$$

where j is current density in the discharge, e is electron charge, and V_{dr} is the electron drift velocity.

The electron drift velocity was determined from the following expression:

$$V_{\text{dr}} = \mu_e E,$$

where μ_e is the electron mobility and E is plasma field strength.

Plasma field strength E is calculated according to the following formula:

$$E = U_{\text{pl}}/d,$$

where U_{pl} is voltage on the plasma and d is the value of the discharge gap.

The average energy of the discharge electrons depends most strongly on the parameter $E/N = 1$–400 Td, while it linearly increases from 0.15 to 8.77 eV. In the parameter range $E/N = 400$–1300 Td, the average electron energy also increases from 8.77 to 29.26 eV but at a lower rate. For the reduced electric field strength range of 615–820 Td, at which experimental studies of the electrical and optical characteristics of the discharge were carried out, the average electron energies

Table 1. Decoding results of the radiation spectrum of a nanosecond discharge between stainless-steel electrodes in air (Fig. 4)

λ, nm	An object	I, arb. units	Lower level	Upper level
208.41	Fe(I)	100	$3d^6 4s^2$	$3d^5(^6\text{S})4s^2 4p$
224.55	Fe(II)	300	$3d^6(^3\text{H})4p$	$3d^6(^3\text{H})4d$
241.78	Fe(II)	60	$3d^6(^3\text{F2})4s$	$3d^6(^3\text{F2})4p$
249.58	Fe(I)	10000	$3d^7(^4\text{F})4s$	$3d^6(^3\text{H})4s4p\ (^3\text{P}^0)$
253.68	Fe(II)	2000	$3d^6(^3\text{H})4s$	$3d^6(^3\text{H})4p$
272.80	Fe(I)	4000	$3d^7(^4\text{F})4s$	$3d^6(^3\text{F2})4s4p(^3\text{P}^0)$
309.15	Fe(I)	120	$3d^7(^4\text{F})4s$	$3d^6(^5\text{D})4s4p(^1\text{P}^0)$

varied within 12.6–16.5 eV. And their highest energies corresponded to values of 177–300 eV.

The results of calculating the average electron energies allow us to determine their temperature in the gas-discharge plasma of the emitter according to the well-known formula [19]:

$$\varepsilon = 3/2\,kT,$$

where ε is the electron energy, k is the Boltzmann constant, and T is the temperature in degrees Kelvin.

It increases from 146160 to 191400 K with a change in the parameter E/N from 615 to 820 TD, respectively.

The mobility of electrons, as follows from the data of numerical calculation, varies within $1.1130 \times 10^{24}N$–$1.03 \times 110^{24}N$ (1/m/V/s) when changing a parameter E/N in the range of 615–820 Td, which gives the electron drift velocity of 6.8×10^4 and 8.4×10^4 m/s, respectively, for the plasma field strength of 15.0×10^6 and 20.0^6 V/m; the electron concentration is 70.3×10^{21}–56.9×10^{21} m^{-3} at a current density of 765×10^6 A/m^2 on the surface of the electrode of the radiation source (0.196×10^{-6} m^2).

Under the conditions of this experiment, the main mechanism for the entry of zinc, copper, and iron vapors into the plasma is the ecton one (explosion of micropoints on the surface of the electrodes), in which the electron density in the discharge can reach 10^{16}–10^{17} cm^{-3} [20]. Therefore, an important contribution to the mechanism of formation of excited atoms and transition metal ions can be introduced by the processes of excitation of metal ions in the ground state by electrons as well as electron-ion recombination processes. The effective cross sections of these processes, for example, for zinc and cadmium ions, are quite large and reach 10^{-16} cm^2 [21].

CHARACTERISTICS OF THIN NANOSTRUCTURED FILMS BASED ON ZINC, COPPER, AND IRON OXIDES

Let us consider the main results into the study of the characteristics of nanostructures based on zinc, copper, and iron oxides that were deposited on a glass substrate near the discharge gap.

Figure 5 shows a photograph of the surface of a film deposited on a glass substrate from the erosion products of copper electrodes and the products of dissociation of air molecules in an overstressed nanosecond discharge. All studies of the synthesis and optical characteristics of the films were carried out at an interelectrode distance of 1 mm. To determine the size of nanostructures, a gel was applied on the film surface based on standard spherical gold nanostructures with a diameter of 20 nm (they are highlighted in yellow in color photographs). Comparative analysis of the sizes of spherical gold nanostructures and of nanostructures synthesized from products of an overstressed nanosecond discharge between copper electrodes in air showed that the sizes of synthesized nanostructures are in the range of 2–20 nm. The transverse dimensions of zinc oxide-based nanostructures were in the range of 2–50 nm, but the formation of large zinc agglomerates with sizes of 1–10 μm was also observed. At increased air pressure and a high energy input into the plasma (when nanosecond discharges are used in the synthesis of nanostructures in a liquid or air), the predominant formation of nanowhiskers or nanostructures of transition metal oxides of a more complex shape is observed [22]. This was confirmed by studying the Raman spectra of laser radiation with a wavelength of 514.5 nm by nanostructures of zinc and copper oxides synthesized in the discharge under study and comparing them with the corresponding Raman spectra of nanowhiskers from other researchers. Thus, in [22], zinc oxide nanostubes were obtained as a result of the action of a high-power, gas-discharge laser based on KrF molecules, which emitted at a wavelength of 248 nm on the surface of a ceramic target made of ZnO.

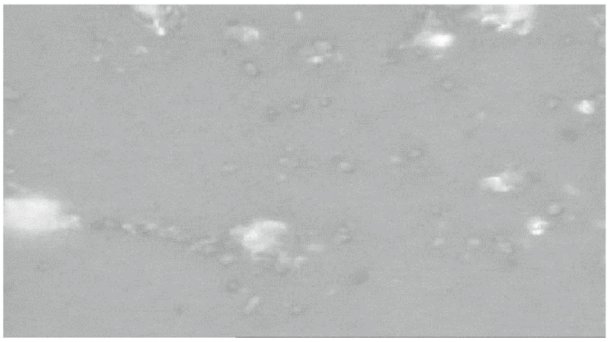

Fig. 5. Surface structure of the film synthesized on a glass substrate from the sputtering products of copper electrodes in atmospheric air in 30 min under the influence of a high-current nanosecond discharge (d = 1 mm and f = 100 Hz).

It can be seen from [23] that the Raman spectrum of radiation scattering of the Ar^+ laser that we registered correlates well with the corresponding spectrum obtained in [22], where Raman scattering of the radiation of the same laser was studied on nanostubes of zinc oxide with a diameter of 8–35 nm. Therefore, we can assume that, under the conditions of the investigated nanosecond discharge, the synthesis takes place of zinc oxide nanostars, which are located perpendicular to the surface of the glass substrate, without the use of transition coatings with nuclei.

Figure 6 shows the transmission spectrum of copper oxide nanostructures. The transmission of such films increased with wave elongation in the visible region of the spectrum and had the appearance of a continuum without maxima and minima in the range from 500 to 650 nm. The results obtained correlate well with the transmission spectrum of copper oxide

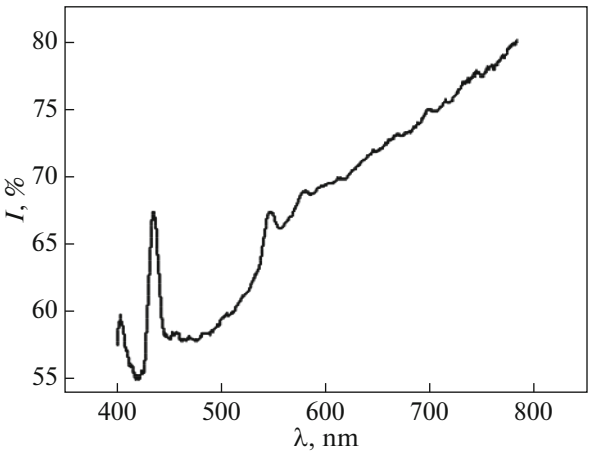

Fig. 6. Transmission spectrum of radiation in the center of the film obtained by sputtering copper electrodes in air for 30 min (d = 1 mm and f = 100 Hz).

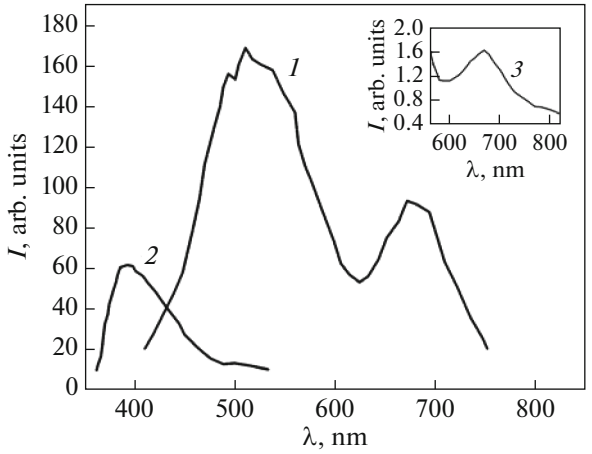

Fig. 7. Photoluminescence spectra of a thin film synthesized by sputtering zinc electrodes in a nanosecond discharge in air, obtained by excitation by radiation of a mercury lamp at wavelengths: (*1*) 270, (*2*) 330, and (*3*) 550 nm.

(Cu_2O) [23]. The absorption band of the film in the wavelength range 550–580 nm corresponds to the absorption band of copper nanostructures [24]. The narrow bands of film clearing in the blue spectral region (at wavelengths of 420 and 450 nm) are probably associated with the action of ultraviolet radiation from the discharge in the spectral range 200–230 nm on the film during its synthesis. The same bleaching bands were observed for films based on zinc oxide. The cause of the appearance of these enlightenment bands may be radiation defects of copper and zinc oxide films as well as the formation of new energy levels in these compounds. The most intense were the transmission bands of nanostructures based on zinc and copper oxides, which correlated with selective and intense plasma radiation of zinc and copper vapors in the 200–230-nm spectral range. In a nanosecond discharge between stainless steel electrodes, the selectivity and intensity of plasma radiation decreased, which led to a decrease in the intensity of the transmission bands in the blue region of the spectrum for nanostructures based on iron oxides [25, 26].

The photoluminescence spectra of zinc oxide-based nanostructures at excitation wavelengths in the range 270–550 nm are shown in Fig. 7. Photoluminescence of the studied nanostructures was most effective under the action of radiation with a wavelength of 330 nm. Photoluminescence of nanostructures in the UV region was practically absent, and it was characterized in the visible region by two broad maxima in the wavelength ranges of 450–480 and 650–680 nm. According to [27], the main mechanism of photoluminescence of zinc oxide nanostructures in the green region is associated with neutral oxygen vacancies, and photoluminescence is determined in the red region by the residual lithium impurity. As the luminescence excitation wavelength increased to the visible spectral region (up to 550 nm), the photoluminescence spectra also shifted to the long-wavelength region, and the photoluminescence intensity decreased significantly. With a decrease in the excitation wavelength from 330 to 270 nm, the luminescence intensity decreased most significantly for the green and red bands.

CONCLUSIONS

It was established that an overstressed nanosecond discharge in atmospheric pressure air between electrodes of transition metals (Zn, Cu) is a selective source of radiation of atoms and ions of zinc and copper in the spectral range 200–230 nm, while plasma radiation was observed for stainless steel electrodes in the spectral range 200–250 nm; at the same time, plasma is a source of flows of molecules and clusters of different compositions based on transition metal oxides, which can be used in microbiology, medicine, and agricultural technologies. When automatically assisted by ultraviolet plasma radiation on glass substrates, thin nanostructured films of zinc and copper oxides are synthesized. They are characterized by transparency windows in the blue spectral region and can be used in optoelectronics.

ACKNOWLEDGMENTS

We are grateful to Senior Researcher Roman Golomb for his help in studying the optical characteristics of nanostructures.

CONFLICT OF INTEREST

The authors declare to have no conflict of interest.

REFERENCES

1. Pakhar'kov, G.P., *Biomeditsinskaya inzheneriya: problemy i perspektivy* (Biomedical Engineering: Problems and Prospects), St. Petersburg: Politekhnika, 2011.
2. Vasilyak, L.M., *Surf. Eng. Appl. Electrochem.*, 2009, vol. 45, no. 1, pp. 26–34.
3. Shuaibov, A.K. and Gritsak, R.V., *Ul'trafioletovi lampi na radikalakh gidroksilu ta eksipleksnikh molekulakh z nakachuvannyam bar'ernim nanosekundnim rozryadom. Monografiya* (Ultraviolet Lamps on Hydroxyl Radicals and Exciplex Molecules Pumped with a Nanosecond Barrier Discharge: Monograph), Uzhgorod: Goverla, 2018.
4. Moshkunov, S.I., Khomich, V.Yu., and Shershunova, E.A., *Tech. Phys. Lett.*, 2018, vol. 44, no. 1, pp. 84–86.
5. Panov, V.A., Vasilyak, L.M., Vetchinin, S.P., Deshevaya, E.A., et al., *Plasma Phys. Rep.*, 2019, vol. 45, no. 5, pp. 517–521.
6. Shuaibov, A.K., Minya, A.I., Gomoki, Z.T., Danylo, V.V., and Pinzenik, P.V., *Surf. Eng. Appl. Electrochem.*, 2019, vol. 55, no. 1, pp. 65–69.
7. Shuaibov, A., Minya, A., Malinina, A., Malinin, A., et al., *Adv. Nat. Sci. Nanosci. Nanotechnol.*, 2018, vol. 9, art. ID 035018.
8. Shuaibov, A., Minya, A., Gomoki, Z.T., and Danylo, V.V., UA Patent 05112, *Byull. Izobret.*, 2017, no. 21.
9. Egorova, E.M., *Biologicheskie effekty nanochastits metallov* (Biological Effects of Metal Nanoparticles), Moscow: Nauka, 2014.
10. Zatolokin, V.D. and Moshkin, A.S., *Vestn. Eksp. Klin. Khir.*, 2010, vol. 3, no. 1, pp. 44–51.
11. Shut, V.N., Mozzharov, S.E., and Yanchenko, V.V., *Vestn. Vitebsk. Gos. Tekhnol. Univ.*, 2016, vol. 31, no. 2, pp. 97–105.
12. Chung, S.H., Hoffman, A., Bader, S.D., Liu, C., et al., *Appl. Phys. Lett.*, 2004, vol. 85, no. 14, pp. 2971–2973.
13. Rozhkova, E.A., Novosad, V., Kim, D.H., Pearson, J., et al., J. Appl. Phys., 2009, vol. 105, art. ID 07B306.
14. Shuaibov, A.K., Minya, O.I., Gomoki, Z.T., and Danylo, V.V., UA Patent 201604596, *Byull. Izobret.*, 2016, no. 21.
15. Shuaibov, A., Mynia, O., Chuchman, M., Homoki, Z., et al., *Proc. XIII Int. Conf. "Electronics and Applied Physics," October 24–27, 2017*, Kyiv, 2016, pp. 151–152.
16. Shuaibov, O.K., Minya, O.Y., Chuchman, M.P., Malinina, A.A., et al., *Ukr. J. Phys.*, 2018, vol. 63, no. 9, pp. 790–801.
17. Baksht, E.K., Tarasenko, V.F., Shut'ko, Yu.V., and Erofeev, M.V., *Russ. Phys. J.*, 2012, vol. 54, no. 11, pp. 1276–1279.
18. BOLSIG+ software. https://nl.lxcat.net/solvers/BOLSIG+/.
19. Raizer, Yu.P., *Fizika gazovogo razryada* (Physics of Gas Discharge), Moscow: Nauka, 1987.
20. Mesyats, G.A., *Phys.-Usp.*, 1995, vol. 38, no. 6, pp. 567–590.
21. Ovcharenko, E.V., Imre, A.I., Gomonai, A.N., and Hutych, Yu.I., *J. Phys. B: At., Mol. Opt. Phys.*, 2010, vol. 43, no. 17, pp. 230–234.
22. Kaydashev, V.E., Kaidashev, E.M., Peres, M., Monteiro, T., et al., *Tech. Phys.*, 2009, vol. 54, no. 11, pp. 1607–1611.
23. Zamanova, E.N. and Alieva, L.A., *Fizika*, 2008, vol. 14, no. 3, pp. 194–196.
24. Farmanfarmaei, B., Rashidian Vaziri, M.R., and Hajiesmaeilbaigi, F., *Quant. Electron.*, 2014, vol. 44, no. 11, pp. 1029–1032.
25. Shuaibov, A.K., Minya, A.Y., Malinina, A.A., Malinin, A.N., et al., *Am. J. Mech. Mater. Eng.*, 2018, vol. 2, no. 1, pp. 8–14.
26. Rutberg, F.G., Gusarov, V.V., Kolikov, V.A., Voskresenskaya, I.P., et al., *Tech. Phys.*, 2012, vol. 57, no. 12, pp. 1641–1645.
27. Rodnyi, P.A., Chernenko, K.A., and Venevtsev, I.D., *Opt. Spectrosc.*, 2018, vol. 125, no. 3, pp. 372–378.